International Journal of Science and Engineering Applications
Volume 14-Issue 11, 89 – 94, 2025, ISSN:- 2319 - 7560
DOI: 10.7753/IJSEA1411.1015

Nickel-Substituted $La_{0.2}Sr_{0.8}TiO_{3-\delta}$ for Efficient Methane Utilization

Mohammad Yousefpour
Department of Science
Azad University of Amol
Amol, Iran

Mahnaz Zameni
Department of Computer Science
Azad University of Sari
Sari, Iran

Abstract: The growing global energy demand and the environmental challenges associated with conventional fossil fuels have intensified the pursuit of sustainable and efficient energy conversion technologies. This study focuses on improving the performance of solid oxide fuel cells (SOFCs) through the development of advanced anode materials. While conventional Ni/YSZ cermet anodes exhibit good electrochemical activity, their long-term stability and tolerance to hydrocarbon fuels remain limited. To address these challenges, $La_{0.2}Sr_{0.8}Ti_{0.9}Ni_{0.1}O_{3-\delta}$ (LSTN) perovskite anodes were investigated for the electro-oxidation of methane. The influence of $LaFe_{0.6}Co_{0.4}O_3$ (LFC) and Pd-doped $LaFe_{0.58}Co_{0.37}Pd_{0.05}O_{3-\delta}$ (LFCP) impregnation on the electrochemical performance of LSTN was systematically examined. The LFCP-impregnated LSTN anodes demonstrated enhanced catalytic activity, reduced polarization resistance, and improved overall performance, which are attributed to the uniform dispersion of LFCP nanoparticles within the anode matrix. These findings provide valuable insights into the design and optimization of SOFC anodes for efficient methane electro-oxidation, contributing to the advancement of clean and sustainable energy technologies.

Keywords: solid oxide fuel cell; anode electrode; LSTN; electrochemical impedance spectroscopy; methane oxidation; infiltration

1. Introduction

The growing global energy demand, along with the significant environmental consequences of conventional energy production, has prompted increased research into sustainable and diverse energy solutions [1-7]. Central to these efforts is the enhancement of energy conversion technologies, particularly solid oxide fuel cells (SOFCs) [8-13] and batteries [14]. SOFCs are regarded as highly efficient devices, generating electricity through the electrochemical reaction of gaseous fuels such as hydrogen and its derivatives [15-17]. A distinguishing advantage of SOFCs over other fuel cell systems is their ability to directly process hydrocarbon fuels via internal reforming [18-20]. Methane, as the simplest hydrocarbon molecule, is notable for lacking a C–C bond, which facilitates its direct reforming within SOFCs [21-23]. Additionally, methane's favorable hydrogen-to-carbon ratio allows it to supply a substantial quantity of hydrogen for SOFC anodes.

In standard SOFC systems, Ni/YSZ ($Zr_xY_{1-x}O_2$) cermet is widely employed as the anode material due to its favorable properties, such as low impedance in hydrogen environments and effective catalytic activity for methane steam reforming [24-28]. Nevertheless, several disadvantages are associated with Ni/YSZ, including limited redox stability and an elevated tendency for coking and sulfur poisoning when exposed to hydrocarbon fuels [29, 30]. To address these challenges, alternative ceramic anodes, including double perovskite materials such as $Sr_2Mg_{1-x}Mn_xMoO_{6-\delta}$ [31] and $Sr_2Fe_{1.4}Ni_{0.1}Mo_{0.5}O_{6-\delta}$ [11, 32], lanthanum chromate based perovskites (e.g. $(La,Sr)(Cr,Mn)O_{3-\delta}$) [17], and strontium titanate based perovskites (e.g. $(La,Sr)(Ti)O_{3-\delta}$) [33], have demonstrated promising properties for application in SOFC anodes.

$La_{0.2}Sr_{0.8}Ti_{0.9}Ni_{0.1}O_{3-\delta}$ (LSTN) perovskite anodes demonstrate enhanced stability and electrochemical performance in both hydrogen and methane atmospheres, with optimized Ni ex-solution and microstructure achieved by controlling firing temperature and atmosphere [34]. Park and Choi [34] showed that LSTN fired at 1250 °C in H2 exhibited the best performance for ScSZ electrolyte-supported cells, combining favorable microstructure with Ni ex-solution to achieve maximum power densities of ~130 mW cm-2 at 800 °C under wet H2. Lee et al. [35] investigated LST infiltration into porous YSZ as SOFC anodes and found that the calcination temperature critically influences the microstructure and electronic conductivity of the LST–YSZ composite. Cells with LST–YSZ anodes calcined at 1373 K exhibited the highest conductivity (>0.4 S/cm) and better electrochemical performance compared to higher temperature calcination due to less sintering and greater porous connectivity [35].

Alongside advances in thin-film fabrication for tailoring the properties of electrode materials [9, 36, 37], one of the most established and effective strategies for enhancing SOFC electrode performance is the impregnation of nanoparticles—typically oxides or noble metals—into the electrode matrix [17, 25, 38, 39]. Rath et al. [40] conducted a comparative study of the $Sr_2FeMoO_{6-\delta}$ (SFM) anode infiltrated with Pd and with Co–Ni–Mo nanoparticles (0.1:5:1 molar ratio, CNM) under humidified hydrogen conditions. Their results showed that the Pd-infiltrated SFM anode exhibited a slightly higher electrode polarization resistance (0.087 Ω cm2) compared to the CNM-infiltrated SFM (0.060 Ω cm2). More recently, $LaFe_{0.7}Co_{0.3}O_{3-\delta}$ and Pd-doped $LaFe_{0.67}Co_{0.3}Pd_{0.03}O_{3-\delta}$ perovskites have been investigated as symmetric electrode materials for SOFCs [41], exhibiting excellent electrocatalytic activity toward both the hydrogen oxidation and oxygen reduction reactions. At 750 °C, the symmetric $LaFe_{0.7}Co_{0.3}O_{3-\delta}/Sm_{0.2}Ce_{0.8}O_{1.9}$ (SDC) and $LaFe_{0.67}Co_{0.3}Pd_{0.03}O_{3-\delta}$/SDC cells achieved power densities of 291 and 535 mW cm^{-2}, respectively. Moreover, Pd incorporation was found to markedly enhance the catalytic activity of $LaFe_{0.7}Co_{0.3}O_{3-\delta}$ for the H_2 oxidation reaction.

In this study, the electro-oxidation of methane on the LSTN anode was systematically examined. To improve the performance of the LSTN electrode, the effects of $LaFe_{0.6}Co_{0.4}O_3$ (LFC) and Pd-doped $LaFe_{0.58}Co_{0.37}Pd_{0.05}O_{3-\delta}$

(LFCP) perovskite structures were thoroughly investigated. The mechanism of methane oxidation on the modified anode was analyzed through comprehensive electrochemical measurements, and both the pristine and impregnated samples were characterized using detailed microstructural analyses.

2. Materials and Methods

Electrolyte pellets were prepared using 8 mol % yttria-stabilized zirconia (YSZ) powder sourced from Tosoh, Japan. The YSZ powders were formed into pellets via cold pressing and subsequently sintered at 1300 °C for 8 hours. The resulting electrolyte pellets had an approximate diameter of 20 mm and a thickness of 0.7 mm. For use as the counter electrode, platinum paste was applied to the center region of each pellet, covering a surface area of 0.5 cm^2. In addition, a ring-shaped reference electrode was implemented. Both the counter and reference electrodes were exposed to air and heat-treated at 900 °C for 1 hour.

For the anode electrode, LSTN powder was combined with Ink Vehicle to form a homogeneous slurry, which was then deposited on the side of the electrolyte opposite the counter electrode. This layer was sintered at 1200 °C for 1 hour in air, generating an anode approximately 0.5 cm^2 in area and 35 µm thick.

LFC and LFCP impregnation solutions were synthesized by dissolving precise stoichiometric amounts of $La(NO_3)_3{\cdot}6H_2O$, $Fe(NO_3)_3{\cdot}9H_2O$, $Co(NO_3)_2{\cdot}6H_2O$, and $Pd(NO_3)_2$ (all from Merck, Germany) in water at a molar ratio of 1:0.6:0.4:0 for LFC and 1:0.58:0.37:0.05 for LFCP, respectively, and adjusting both solutions to a concentration of 0.3 M. Ethylene glycol (EG) was added in a 2.4:1 M ratio as a complexing agent. A drop of LFC or LFCP solution was carefully deposited on the LSTN anode surface, dried in air, and blotted with a tissue. Subsequent heat treatment was conducted at 900 °C for 2 hours in air.

Drying of the LFC and LFCP solutions was completed in an oven, followed by calcination at 900 °C for 2 hours in air, using the protocol of Rostaghi Chalaki et al. [34]. The resulting phase composition of LFC and LFCP powders was assessed by X-ray diffraction (XRD) at room temperature using a Philips PW 1730 diffractometer (Cu-Kα, λ=1.5406 Å), with 2θ spanning 20–80° at 0.02° increments. The microstructural features of the impregnated LSTN anodes were examined by field emission scanning electron microscopy (FESEM) using a TESCAN MIRA3.

For electrochemical characterization, a three-electrode configuration was employed. Platinum paste was applied to the anode surface as a current collector, with platinum wires used for electrical contacts. Methane served as the fuel, and both the counter and reference electrodes were maintained in air. Prior to testing, the anodes were activated in methane at 850 °C for one hour. Electrochemical impedance spectroscopy (EIS) was performed at open circuit potential (OCP) from 0.01 Hz to 100 kHz using a PGSTAT302N Autolab analyzer, while the Zsimpwin software package was used to extract the electrode polarization (R_E) and ohmic resistances (R_Ω).

3. Result and Discussion

Figure 1 displays the X-ray diffraction (XRD) results for LFC and LFCP powders after calcination at 900 °C in air. The pattern obtained for the calcined LFC powder closely matches the reference pattern for $LaFe_{0.6}Co_{0.4}O_3$ (JCPDS card no. 00-044-0361), confirming phase purity without detectable impurities. For the LFCP sample, the XRD peaks are shifted to lower angles relative to LFC, reflecting a reduction in interplanar spacing resulting from Pd incorporation. These findings demonstrate that perovskite phases of both LFC and LFCP can successfully form within the porous structure of the LSTN anode after impregnation and thermal treatment of LFC and LFCP solutions.

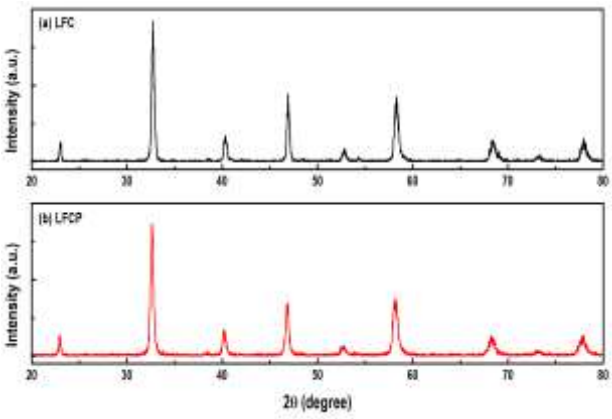

Figure 1. XRD patterns of LFC and LFCP solutions calcined at 900 °C for 2 h in air.

Figure 2 presents the impedance spectra recorded for the LSTN anode measured at open-circuit potential across various temperatures under methane fuel. Spectral analysis employed an equivalent circuit model, $R_\Omega(R_hQ_h)(R_mQ_m)(R_lQ_l)$, where R_Ω denotes the cell's ohmic resistance. The terms R_h, R_m, and R_l correspond to electrode polarization resistances (summed as $R_E = R_h + R_m + R_l$), and Q_h, Q_m, Q_l represent the constant phase elements linked to the respective high, medium, and low-frequency arcs.

During methane oxidation at 750 °C, the electrode polarization resistance was found to be 15.81 Ω cm^2, which decreased to 11.91 Ω cm^2 at 800 °C and further reduced to 7.30 Ω cm^2 at 850 °C. These results are summarized in Table 1. Analysis of the activation energy associated with the distinct frequency arcs revealed values of 1.08 eV (high frequency), –0.069 eV (medium frequency), and 0.77 eV (low frequency), respectively. The positive activation energies for the high- and low-frequency arcs indicate thermally activated processes, while the negative value for the medium-frequency arc suggests slight thermal deactivation in this regime.

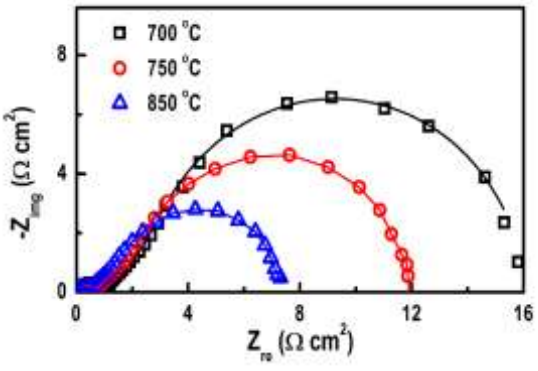

Figure 2. LSTN anode electrode polarization resistance at 750, 800, and 850 °C in methane. Points are experimental data and solid lines are fitted data with the equivalent circuit RΩ(RQ)1(RQ)2(RQ)3.

At 850 °C, the high-frequency arc was observed at 2511 Hz and had an activation energy of 1.04 eV. In studies of methane oxidation on the LLSTN/YSZ composite anode in wet methane, Jiang et al. [42] reported three distinctive impedance

International Journal of Science and Engineering Applications
Volume 14-Issue 11, 89 – 94, 2025, ISSN:- 2319 - 7560
DOI: 10.7753/IJSEA1411.1015

arcs and linked the high-frequency arc to transfer of charged species at the LLSTN/YSZ interface. In another investigation comparing $La_{0.4}Sr_{0.6}Ti_{1-x}Mn_xO_{3-\delta}$ (LSTM) to LSTM/YSZ composite anodes, the latter exhibited a much smaller high-frequency arc, attributed to a substantially increased LSTM/YSZ interface area and enhanced charge transfer. Given the similar characteristics seen in this work and previous results [43], the high-frequency arc here is taken to reflect charge transfer processes in the LSTN anode.

Primdahl and Mogensen [44] Primdahl and Mogensen investigated electrochemical oxidation of wet H_2 on Ni/YSZ at 1000 °C in a three-electrode configuration, recording an arc with a summit frequency near 1 Hz and a small negative activation energy (–0.09 eV), which they assigned to gas conversion at the anode surface. With a different fuel composition for the anode compared to the counter and reference electrodes in the present study, the medium-frequency arc at 850 °C peaks at 0.9 Hz and has an activation energy of –0.069 eV. In line with previous findings [43, 44], the medium-frequency arc is attributed to gas-phase conversion at the surface of the LSTN anode.

Jiang et al. [45] examined impedance behavior of a Ni/YSZ anode operating in moist H_2 at 850 °C and identified a low-frequency arc at 0.02 Hz with a 0.42 eV activation energy, assigning it to hydrogen dissociative adsorption on Ni particles. Since the low-frequency arc in this study is thermally activated and peaks at 0.87 Hz at 850 °C, it is similarly associated with hydrogen dissociative adsorption on the LSTN anode.

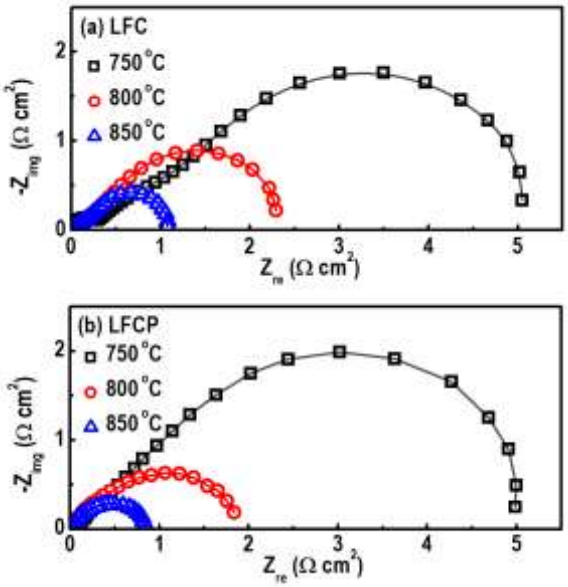

Figure 3. Impedance spectra of LSTN anodes impregnated with (a) LFC and (b) LFCP at 750, 800, and 850 °C in methane. Points are experimental data and solid lines are fitted data with the equivalent circuit $R_\Omega(R_hQ_h)(R_mQ_m)(R_lQ_l)$.

Figure 3 demonstrates how treating the LSTN electrode with LFC and LFCP solutions improves its performance under methane at various temperatures. At 750 °C, the polarization resistance fell from 15.81 to 5.05 and 4.98 Ω cm² after impregnation with LFC and LFCP, respectively. When increased to 800 °C, resistance dropped from 11.91 to 2.29 and 1.96 Ω cm² for LFC and LFCP, respectively. This reduction continued at 850 °C, decreasing from 7.30 to 1.07 and 0.86 Ω cm² with these solutions. Across all temperatures tested, LFCP showed more substantial improvements than LFC, probably owing to higher activity of Pd ions in the perovskite network. The particularly large resistance drop at 850 °C is attributed to enhanced catalytic activity of LFC and LFCP perovskites at elevated temperatures.

The polarization resistance of the LSTN anode during methane electro-oxidation showed a significant decrease after impregnation with both solutions. This improvement was primarily due to notable reductions in the medium- and low-frequency regions [46]. The lowered polarization resistance at low frequencies likely stems from enhanced catalytic activity for hydrogen adsorption, facilitated by both impregnation treatments. In the medium-frequency domain, LFCP impregnation led to a more pronounced reduction in polarization resistance compared to LFC, possibly due to the greater catalytic efficiency of LFCP in methane decomposition [47]. Conversely, the application of LFC resulted in a substantial decrease in polarization resistance at high frequencies, likely related to improved ionic conduction within the anode. Collectively, these results suggest that LFCP impregnation significantly influences polarization resistance across all three frequency arcs.

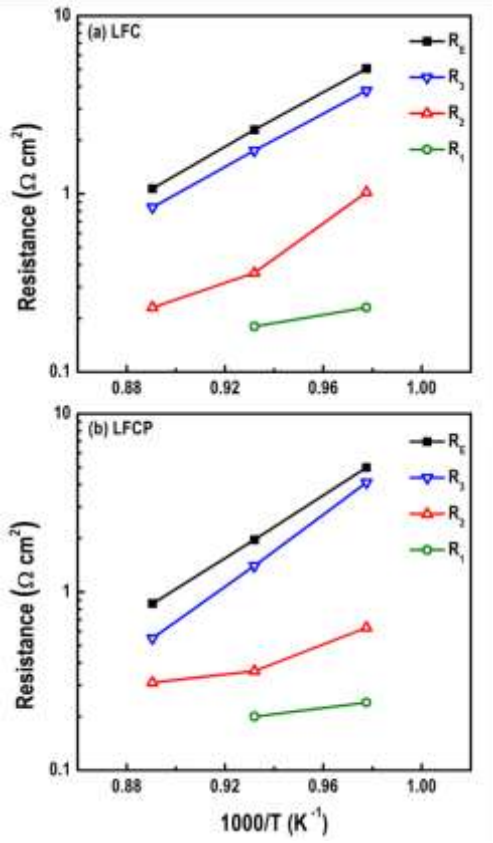

Figure 4. Effect of (a) LFC and (b) LFCP solutions impregnation on R_1, R_2, R_3, and RE of LSTN anode at 750, 800, and 850 °C in methane.

SEM images in Figure 5 clearly show morphological changes in the LSTN anode before and after treatment with LFC and LFCP. After impregnation, distinct nanoparticles appeared on the anode surface, with LFCP-treated samples displaying a more prominent formation compared to LFC. Consistent with the electrochemical results, LSTN anodes infiltrated with LFCP presented lower polarization resistance than those treated with LFC. This enhanced performance can be attributed to the uniform dispersion and well-developed incorporation of LFCP nanoparticles within the porous structure of the LSTN anode.

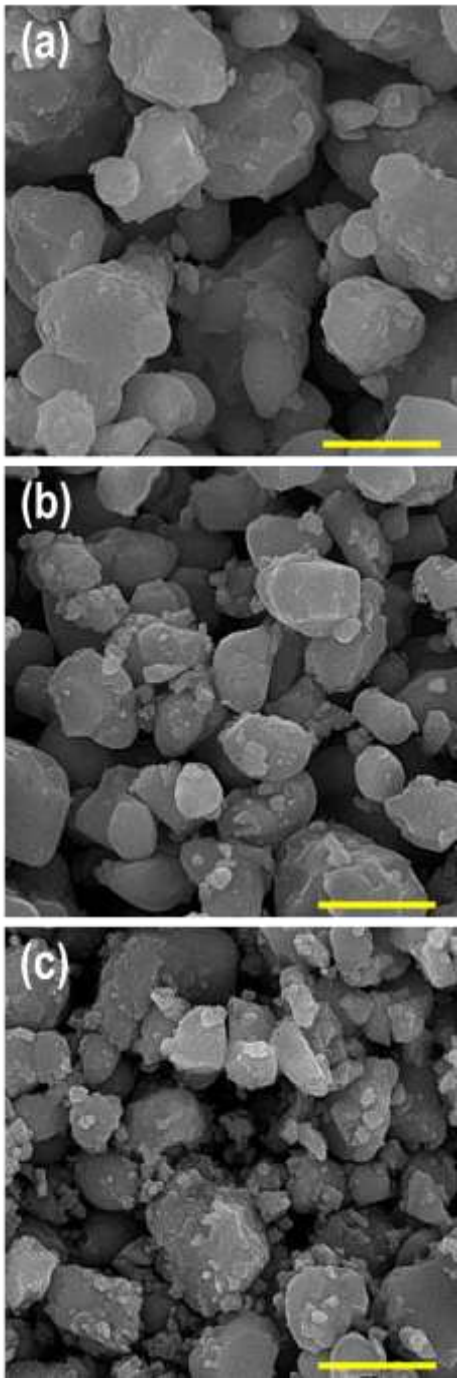

Figure 5. SEM micrograph of LSTN anode electrode, (a) before, and after (b) LFC (c) and (d) LFCP solution impregnation.

4. Conclusion

The LSTN anode exhibited a relatively high electrode polarization resistance during methane oxidation at 850 °C. Analysis of the impedance spectra using an equivalent circuit model indicated that the electro-oxidation of methane on the LSTN anode is governed by at least three distinct electrode processes: high-frequency charge transfer, medium-frequency gas conversion, and low-frequency hydrogen dissociative adsorption. The polarization resistance of the LSTN anode was significantly reduced following impregnation with LFC solution. The presence of LFC nanoparticles enhanced the electrocatalytic activity by promoting methane decomposition and hydrogen adsorption. Furthermore, Pd doping within the LFC perovskite structure (LFCP) led to an even greater improvement in electrode performance, with the low-frequency polarization resistance decreasing more substantially for LFCP-impregnated anodes than for those modified with LFC.

5. Acknowledgments

The author would like to thank the Azad University of Amol. This study did not receive funding from any government or private agency.

6. References

[1] Taghavi, H., Liquid Cooling System for a High Power, Medium Frequency, and Medium Voltage Isolated Power Converter. 2023, University of South Carolina: United States -- South Carolina. p. 74.

[2] Bhuvela, P., H. Taghavi, and A. Nasiri. Design Methodology for a Medium Voltage Single Stage LLC Resonant Solar PV Inverter. in 2023 12th International Conference on Renewable Energy Research and Applications (ICRERA). 2023. IEEE.

[3] Taghavi, H., A. El Shafei, and A. Nasiri. Liquid Cooling System for a High Power, Medium Frequency, and Medium Voltage Isolated Power Converter. in 2023 12th International Conference on Renewable Energy Research and Applications (ICRERA). 2023. IEEE.

[4] Bhuvela, P., H. Taghavi, and A. Nasiri, Loss Analysis of a Resonant Converter Based Medium Voltage Single Stage Solar PV Inverter. IEEE Transactions on Industry Applications, 2025.

[5] Taghavi, H., et al. Design and Optimization of a Forced-Air Cooling System for a Compact Medium Voltage Solar Photovoltaic Inverter. in 2024 13th International Conference on Renewable Energy Research and Applications (ICRERA). 2024. IEEE.

[6] Taghavi, H., S. Raghu, and J.A. Khan. Optimization of Thermal Management in Power Electronics by the Design of Split Channel Cooling Systems Through Numerical Simulations. in Heat Transfer Summer Conference. 2024. American Society of Mechanical Engineers.

[7] Bhuvela, P., H. Taghavi, and A. Nasiri. 13.8 kV, 1MW Resonant Direct AC Medium Voltage Single Stage Solar PV Inverter. in 2024 IEEE Applied Power Electronics Conference and Exposition (APEC). 2024. IEEE.

[8] Fan, L., et al., Nanomaterials and technologies for low temperature solid oxide fuel cells: recent advances, challenges and opportunities. Nano Energy, 2018. 45: p. 148-176.

[9] Yang, G., et al., Tuning Ionic Conductivity in Fluorite Gd-Doped CeO2-Bixbyite RE2O3 (RE= Y and Sm) Multilayer Thin Films by Controlling Interfacial Strain. ACS Applied Electronic Materials, 2023. 5(8): p. 4556-4563.

[10] Li, H., et al., Unlocking the Potential of A-Site Ca-Doped LaCo0. 2Fe0. 8O3− δ: A Redox-Stable Cathode Material Enabling High Current Density in Direct CO2 Electrolysis. ACS Applied Materials & Interfaces, 2023. 15(37): p. 43732-43744.

[11] Wang, M., et al., Improved Solid-State Reaction Method for Scaled-Up Synthesis of Ceramic Proton-Conducting Electrolyte Materials. ACS Applied Energy Materials, 2023. 6(15): p. 8316-8326.

[12] Lin, J., et al., Atmospheric plasma spraying to fabricate metal-supported solid oxide fuel cells with open-channel

porous metal support. Journal of the American Ceramic Society, 2023. 106(1): p. 68-78.

[13] Nakhi, A., et al., Unveiling the Promoted LSTM/YSZ Composite Anode for Direct Utilization of Hydrocarbon Fuels. International Journal of Science and Engineering Applications, 2023. 12(12): p. 18 - 24.

[14] Jeena, M., et al., A siloxane-incorporated copolymer as an in situ cross-linkable binder for high performance silicon anodes in Li-ion batteries. Nanoscale, 2016. 8(17): p. 9245-9253.

[15] Lee, K.T. and E.D. Wachsman, Role of nanostructures on SOFC performance at reduced temperatures. Mrs Bulletin, 2014. 39(9): p. 783-791.

[16] Park, K.-Y., et al., High-performance Ruddlesden–Popper perovskite oxide with in situ exsolved nanoparticles for direct CO 2 electrolysis. Journal of Materials Chemistry A, 2023. 11(39): p. 21354-21364.

[17] Rostaghi Chalaki, H., et al., LaFe 0.6 Co 0.4 O 3 promoted LSCM/YSZ anode for direct utilization of methanol in solid oxide fuel cells. Ionics, 2020. 26: p. 1011-1018.

[18] Ge, X.M., et al., Solid oxide fuel cell anode materials for direct hydrocarbon utilization. Advanced Energy Materials, 2012. 2(10): p. 1156-1181.

[19] Wang, W., et al., Improving the performance for direct electrolysis of CO 2 in solid oxide electrolysis cells with a Sr 1.9 Fe 1.5 Mo 0.5 O 6− δ electrode via infiltration of Pr 6 O 11 nanoparticles. Journal of Materials Chemistry A, 2023. 11(16): p. 9039-9048.

[20] Park, K.-Y., et al. A Highly Performing Electrode with in-Situ Exsolved Nanoparticles for Direct Electrolysis of CO2. in Electrochemical Society Meeting Abstracts 242. 2022. The Electrochemical Society, Inc.

[21] Abbas, H.F. and W.W. Daud, Hydrogen production by methane decomposition: a review. International journal of hydrogen energy, 2010. 35(3): p. 1160-1190.

[22] Wang, M., et al., Nanostructured carbon as highly efficient and stable anodes for ethylene production and power generation in protonic ceramic electrochemical cells. Carbon, 2022. 199: p. 379-386.

[23] Sun, R., et al., Crystallization Behavior and Luminescence of Inkjet Printing CH3NH3PbBr3. Crystal Research and Technology, 2021. 56(8): p. 2100004.

[24] McIntosh, S. and R.J. Gorte, Direct hydrocarbon solid oxide fuel cells. Chemical reviews, 2004. 104(10): p. 4845-4866.

[25] Chalaki, H.R., et al. The Effect of Impregnation of Ceramic Nano-particles on the Performance of LSCM/YSZ Anode Electrode of Solid Oxide Fuel Cell. in 5th International Conference on Materials Engineering and Metallurgy. 2016.

[26] Wang, W., et al. Rational Identification of Doping Strategy to Achieve a Highly Conductive and Reliable Protonic Electrolyte for Electrochemical Cells. in Electrochemical Society Meeting Abstracts 239. 2021. The Electrochemical Society, Inc.

[27] Du, Y., et al., Preparation and thermoelectric properties of graphite/poly (3, 4-ethyenedioxythiophene) nanocomposites. Energies, 2018. 11(10): p. 2849.

[28] Jia-Yue, X., et al., Growth and characterization of all-inorganic perovskite CsPbBr3 crystal by a traveling zone melting method. Journal of Inorganic Materials, 2018. 33(11): p. 1253-1258.

[29] Su, C., et al., Progress and prospects in symmetrical solid oxide fuel cells with two identical electrodes. Advanced Energy Materials, 2015. 5(14): p. 1500188.

[30] Li, H., et al. C2H6 Dehydrogenation and Electrical Power Production in a Protonic Conducting Fuel Cell with in-Situ Exsolved Metal Nanoparticle Catalyst. in Electrochemical Society Meeting Abstracts 239. 2021. The Electrochemical Society, Inc.

[31] Huang, Y.-H., et al., Double perovskites as anode materials for solid-oxide fuel cells. Science, 2006. 312(5771): p. 254-257.

[32] Li, H., et al. A-Site Doping Effect on the Performance of Sr2Fe1. 4 Ni0. 1Mo0. 5O6-Δ Anodes for SOFCs. in Electrochemical Society Meeting Abstracts 242. 2022. The Electrochemical Society, Inc.

[33] Marina, O.A., N.L. Canfield, and J.W. Stevenson, Thermal, electrical, and electrocatalytical properties of lanthanum-doped strontium titanate. Solid State Ionics, 2002. 149(1-2): p. 21-28.

[34] Park, B.H. and G.M. Choi, Effect of anode firing on the performance of lanthanum and nickel co-doped SrTiO3 (La0. 2Sr0. 8Ti0. 9Ni0. 1O3− δ) anode of solid oxide fuel cell. Journal of Power Sources, 2015. 293: p. 684-691.

[35] Lee, S., et al., SOFC anodes based on infiltration of La0. 3Sr0. 7TiO3. Journal of the Electrochemical Society, 2008. 155(11): p. B1179.

[36] El Loubani, M., et al., Creation of submicron-scale metal oxide speckle patterns on single carbon fibers by a thermodynamically and kinetically controlled nonequilibrium process. Materials & Design, 2025. 250: p. 113582.

[37] Loubani, M.E., et al., Multifunctional Electrocatalysts for Low-temperature Solid Oxide Fuel Cells. 2024.

[38] Shirvani, S.M.N., et al., Optimal design of a composite sandwich panel with a hexagonal honeycomb core for aerospace applications. Iranian Journal of Science and Technology, Transactions of Mechanical Engineering, 2023. 47(2): p. 557-568.

[39] Seyed Mostafa Nasrollahpour Shirvani, M.G., Hamed Afrasiab, Ramazanali Jafari Talookolaei, Optimization of a Composite Sandwich Panel with Honeycomb Core Under Out-of-Plane Pressure with NMPSO Algorithm, in The 28th Annual International Conference of Iranian Society of Mechanical Engineers (ISME). 2020.

[40] Rath, M.K. and K.-T. Lee, Superior electrochemical performance of non-precious Co-Ni-Mo alloy catalyst-impregnated Sr2FeMoO6-δ as an electrode material for symmetric solid oxide fuel cells. Electrochimica Acta, 2016. 212: p. 678-685.

[41] Shen, J., et al., Impregnated LaCo0. 3Fe0. 67Pd0. 03O3-δ as a promising electrocatalyst for “symmetrical” intermediate-temperature solid oxide fuel cells. Journal of Power Sources, 2016. 306: p. 92-99.

[42] Jiang, S.P., et al., (La0. 75Sr0. 25)(Cr0. 5Mn0. 5) O3/YSZ composite anodes for methane oxidation reaction in solid oxide fuel cells. Solid State Ionics, 2006. 177(1-2): p. 149-157.

[43] Fu, Q., F. Tietz, and D. Stöver, La0. 4Sr0. 6Ti1− x Mn x O3− δ perovskites as anode materials for solid oxide fuel

cells. Journal of the Electrochemical Society, 2006. 153(4): p. D74.

[44] Primdahl, S. and M. Mogensen, Gas conversion impedance: a test geometry effect in characterization of solid oxide fuel cell anodes. Journal of the electrochemical Society, 1998. 145(7): p. 2431.

[45] Jiang, S., W. Wang, and Y. Zhen, Performance and electrode behaviour of nano-YSZ impregnated nickel anodes used in solid oxide fuel cells. Journal of power sources, 2005. 147(1-2): p. 1-7.

[46] Yousefpour, K., et al. *Control of Grid-Connected Inverters Using PLL for Synchronization and Harmonic Mitigation*. in *2025 IEEE Texas Power and Energy Conference (TPEC)*. 2025. IEEE.

[47] Varnousfaderani, S.A., et al. *Real-World Evaluation of Compressed Sensing for Data Compression in Smart Grids*. in *2025 IEEE Texas Power and Energy Conference (TPEC)*. 2025. IEEE.